

A Feasibility Study of Tissue Characterization Using Implanted LC Sensors

Marie Yvanoff, *Student Member, IEEE*, and Jayanti Venkataraman, *Senior Member, IEEE*

Abstract— Bio-implantable sensors using RF telemetry links, that enable the continuous monitoring and recording of physiological data, are receiving a great deal of attention. The objective of the present work is to study the feasibility of an implantable sensor for tissue characterization. This has been done by querying an LC sensor surrounded by dispersive tissues by an external antenna. The resonant frequency of the sensor is monitored by measuring the input impedance of the antenna, and correlated to the desired quantities. Using an equivalent circuit model of the sensor that accounts for the properties of the encapsulating tissue, analytical expressions have been developed for the extraction of the tissue permittivity and conductivity. Finally, experimental validation has been performed with a telemetry link that consists of a loop antenna and a fabricated LC sensor immersed in single and multiple dispersive phantom materials.

Index Terms— Biological tissue, Interdigital Capacitor, LC-sensor, RF Telemetry.

I. INTRODUCTION

Over the past few decades, there has been growing interest and research on bioimplantable devices using RF telemetry links. Externally powered implantable devices using inductive coupling are now being used to provide RF links between the internal device and the outside equipment. They also enable to continuously monitor and record physiological data. As an example, the progress to date in the development of implantable biosensor systems can be found in [1].

In a typical biotelemetry system, a loop antenna is shown to present good coupling and power deposition with an orientation parallel to the body [2]. RF telemetry concepts for implantable micro-inductors have been validated in the presence of tissue-like phantoms [3]. However, the effect of multiple layers of tissue and inhomogeneity has not been analyzed to date and the dispersive properties of tissues make this a formidable task. The effects of layered biological tissues on a biotelemetry link have been studied in [4] and the shift in resonant frequency due to the dispersive media encapsulating an LC sensor has also been demonstrated.

In the present work, a novel technique for tissue characterization using an LC sensor is developed which allows for the extraction of the relative permittivity, and the conductivity of dispersive tissues. The use of an

interdigital capacitor in the sensor allows for tissue characterization since the dielectric properties of the tissue in which it is embedded will affect its impedance and resonant frequency [5]. Biological tissue can be modeled using available data derived from extensive work in compiling measurements from tissues [6-8]. The implanted sensor communicates with a loop antenna via mutual inductive coupling. The method is based on querying the sensor when embedded in layered tissue with an external antenna (Fig.1). From the measurement of the input impedance Z_{in} of the antenna, the resonant frequency and the input impedance of the sensor are obtained.

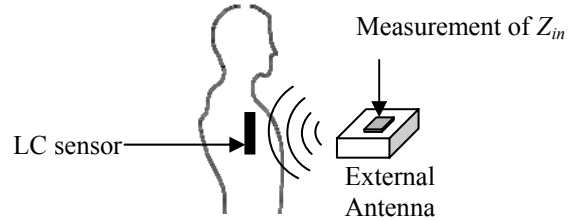


Fig. 1. RF Telemetry.

The capacitor saturation is first studied as a function of the number, and thickness, of tissue layers present. A saturation thickness is defined, which allows for the sensor to be implanted at a depth where it is only affected by the properties of the layer in which it is embedded. It is demonstrated that all other layers over it do not affect the resonant frequency or input impedance of the sensor. Using an equivalent circuit model of the sensor that accounts for the properties of the encapsulating tissue, analytical expressions have been developed for the extraction of the tissue permittivity and conductivity.

Experimental studies using phantom tissues are an important step for exploring the feasibility of new techniques for biomedical application. They have been used by many research groups [18,19]. The technique presented in this work is therefore validated with experimentation using dispersive phantom tissue.

II. LC SENSOR DESIGN

A. Sensor Geometry and Equivalent Circuit

The LC sensor consisting of a spiral inductor and an interdigital capacitor (IDC), as shown in Fig. 2, resides on top of a substrate with a relative permittivity, ϵ_{rs} and thickness, d_s . It is covered by a protective layer which is typically, a bio-compatible material such as parylene.

The sensor is embedded in multiple tissue layers. The first tissue layer encapsulating it, referred to henceforth as the sensing layer, has a relative permittivity ϵ_{r1} , conductivity, σ_1 , and thickness d_l . The sensitivity of the sensor will be dependent on its physical geometry, as well as its material properties. The length of the interdigitated fingers is l and the number of finger pairs is N . Both the inductor and capacitor are formed of metal lines, of width w , and spacing s .

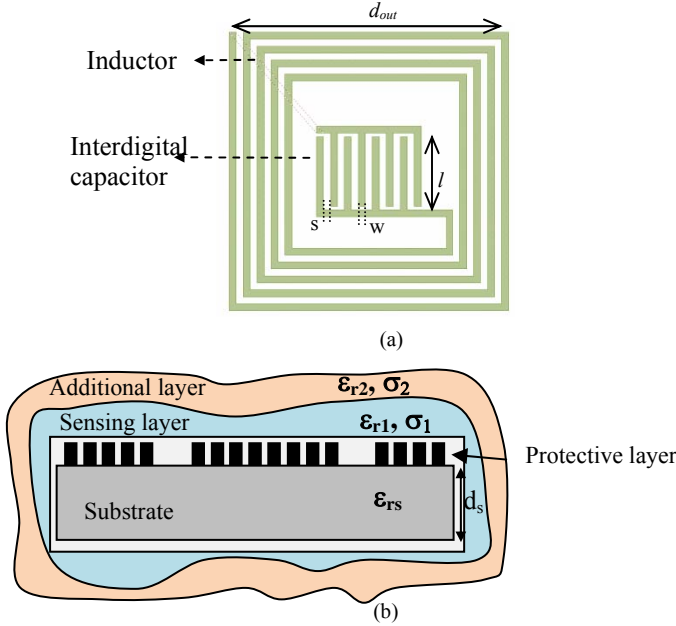


Fig. 2. Planar LC sensor geometry (a) top view (b) cross section.

The inductance L_s of a rectangular planar inductor can be calculated using available expressions [9], as a function of the outer dimension d_{out} , the width w , and spacing s of the lines, and the number of turns. The capacitance C_s is also function of the line width w and spacing s as well as the length of the fingers l , and the number of finger pairs N . It is sensitive to the properties of the dielectric surrounding it, and this is studied in detail.

The equivalent circuit of the sensor, embedded in a lossy dielectric, is shown in Fig.3 where R_{sD} is a resistance due to the conduction current in the lossy material.

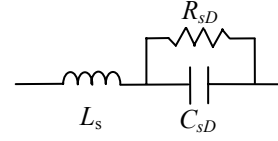


Fig. 3. Equivalent circuit of the sensor inside lossy dielectric [5].

The sensor impedance Z_s of the circuit shown in Fig.3 is given as,

$$Z_s = j\omega L_s + \frac{R_{sD}}{1 + j\omega R_{sD} C_{sD}} \quad (1)$$

Under the saturation condition, the interdigital capacitance and resistance can be approximated as a function of the dielectric permittivity of the substrate ϵ_{rs} , and the biological ‘‘sensing tissue layer’’ properties, ϵ_{r1} and σ_1 [10],

$$C_{sD} = \epsilon_0 (\epsilon_{rs} + \epsilon_{r1}) k \quad (2a)$$

$$R_{sD} = \frac{1}{\sigma_1 k} \quad (2b)$$

where k is function of the spacing, s , the width, w , the length, l , of the fingers and the number of finger pairs, N and is given by (3) [10].

$$k = \frac{1}{2} \left[\frac{K[w/(w+s)]}{K[(1-(w/(w+s))^2)^{1/2}]} \right] l(N-3) \quad (3)$$

where K is the elliptical function of the 1st kind.

From the measurement of the input impedance of an external antenna, a procedure will be demonstrated for obtaining the capacitance C_{sD} and resistance R_{sD} , and therefore extracting the permittivity and conductivity of the sensing layer.

It should be pointed out that human tissue is not homogeneous. However, the interdigital capacitor width w and spacing s and the overall size of the sensor are very small. The sensor can therefore be designed to reduce the thickness of the saturation region to minimize the fringing field around it. This allows us to assume that the region surrounding the sensor is homogeneous. The sensor can be implanted at a certain depth where it will be affected only by the sensing layer. Additional surrounding layers, which may or may not be homogeneous, will not affect its performance.

B. Telemetry System

The RF telemetry system studied here consists of the LC resonant sensor, implanted in multiple layers of tissue, and queried by an external transmitter/receiver loop antenna. Biological tissues can be characterized by their electrical properties and are equivalent to dispersive dielectric materials, where the complex permittivity is defined as

$$\hat{\epsilon}_p(\omega) = \epsilon_p(\omega) + \frac{\sigma(\omega)}{j\omega\epsilon_0}, \quad (4)$$

The electrical properties of tissues vastly differ between organs, and for the same organ, between the diseased and healthy state. This allows for tissue characterization and differentiation by the extraction of the permittivity and conductivity.

The interaction of the external antenna and the sensor is explained via the equivalent circuit model in Fig.4. When the sensor is placed in close proximity to the loop antenna, inductive coupling occurs and it is possible to detect its resonant frequency from the input impedance measurements of the external antenna. The impedance of the sensor is monitored and the resulting shift in the resonant frequency when placed within the tissue is assessed. The impedance of the external antenna coil, in the presence of the sensor, is given as

$$Z_{in}(\omega) = R_a + j\omega L_a + \frac{\omega^2 M^2}{Z_s}, \quad (5)$$

where ω is the angular frequency, M is the mutual inductance, L_a and R_a are the external antenna inductance and resistance, and Z_s is the sensor impedance defined in (1).

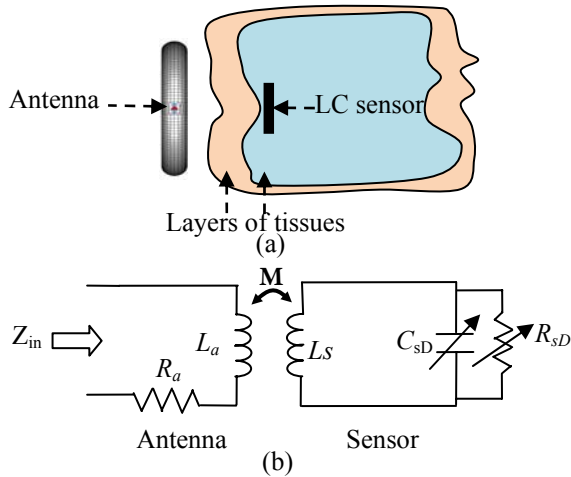


Fig. 4. (a) Telemetry System, (b) Equivalent circuit

In (5), it is seen that by monitoring the input impedance Z_{in} of the external antenna, it is possible to

detect the resonant frequencies of the sensor independent of the value of M . In the analytical formulations and in the simulation model, only the sensor is considered whereas in the experimentation, all measurements are made at the input terminals of the external antenna which queries the sensor. It should be emphasized that a knowledge of the sensor and its geometry is not required.

III. STUDY OF SATURATION CRITERION

A. Capacitor Saturation

For an interdigital capacitor, it is known that as the thickness of the dielectric layer on top of the capacitor increases, the capacitance continues to increase until it reaches its so-called saturation value which is 99.5% of its maximum value. This thickness is referred to as the penetration depth of the fringing fields. The effect of the sensing layer thickness on the capacitor saturation is key to the methodology developed in this paper. The sensor needs to be embedded at a depth in the tissue that ensures that the capacitor has reached its saturation value. Under this condition, the sensor resonant frequency will be affected only by the properties of the first encapsulating layer and will be unaffected by additional surrounding layers.

The capacitance defined in (2), from [10], is for infinite thickness of substrate and sensing layer. It is necessary to study the saturation of the capacitor as a function of the sensing layer thickness d_l and its properties and to extend the analysis for multiple layers of tissue.

A study of the saturation of the capacitor, with respect to the sensing thickness d_l , has been performed through simulation, using SONNET [11], a planar shielded method of moment tool. As an example, a capacitor consisting of 10 fingers is analyzed, Fig.5. Each finger is of length l equal to 2.5 mm, and the width w and spacing s are both equal to $62.5 \mu\text{m}$. The capacitor is on a substrate with thickness $d_s = 787 \mu\text{m}$, and permittivity ($\epsilon_{rs}=2.33$). In this case, the sensing layer is a lossy material with permittivity ϵ_{r1} and conductivity σ_1 equal to 80 and 0.5 (S/m) respectively.

The simulated capacitance is shown in Fig. 6 as a function of the sensing layer thickness d_l . As the sensing layer thickness d_l increases, it is observed that the capacitance increases until it reaches saturation.

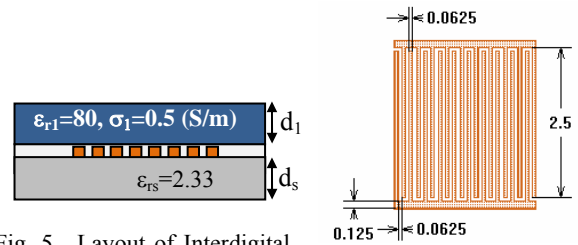


Fig. 5. Layout of Interdigital

capacitor simulated with SONNET (dimensions are in mm).

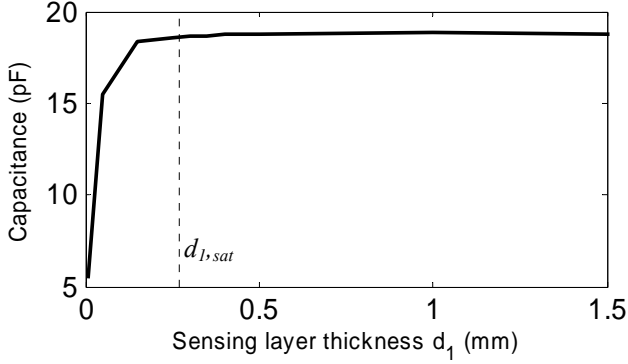


Fig. 6. Interdigital capacitance as a function of d_1 , simulation results with SONNET.

The saturation thickness obtained by simulation agrees well with that obtained from [12], as a constant value, $d_{1,sat}$, which is 0.3 mm for this example, and is marked in the diagram (dotted line).

B. Impact of Saturation Thickness on Sensor Admittance

The impact of the sensing layer thickness on the admittance and resonant frequencies of the sensor is now analyzed. Simulations have been performed with SONNET, to confirm that, after the capacitor in the sensor has saturated, additional tissue layers do not affect its resonant frequency. In Fig. 7, the sensing layer has a relative permittivity ϵ_{r1} equal to 80 and a conductivity σ_1 equal to 0.5 S/m. The impact of the sensing layer thickness d_1 and the second layer thickness, d_2 is studied.

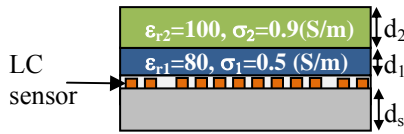


Fig. 7. Cross-section of geometry studied with multiple lossy layers.

The admittance Y_s of the sensor is plotted in Fig. 8 as a function of frequency for varying thicknesses of d_1 . The frequency at which the susceptance becomes zero, referred to as the zero-susceptance frequency $f_{D,z}$, and the frequency corresponding to the maximum of the conductance, $f_{D,max}$ are noted. It can be observed that for a lossy dielectric, $f_{D,z}$ and $f_{D,max}$ are different. However when the dielectric is lossless, they will be the same.

The frequencies $f_{D,max}$ and $f_{D,z}$ are obtained for different thicknesses of d_1 and d_2 , the results are summarized in Table.1. At first setting d_2 as zero, the thickness of the sensing layer d_1 is increased. It is observed that the resonant frequencies of the LC sensor varies until the saturation value $d_{1,sat}$. After saturation has been reached,

the thickness of the sensing layer does not impact the sensor resonant frequencies. At this point, a second layer a thickness d_2 equal to 10 mm with relative permittivity of 100, and conductivity of 0.9 (S/m) is added on top of the sensing layer as shown in Fig.7. Negligible effect is observed on the resonant frequencies of the sensor, as shown in Fig.9 and Table.1.

In summary, the capacitance of the interdigital capacitor increases as the thickness of the encapsulating layer increases until saturation is achieved, at which point it remains constant. This is significant because additional layers can be added without affecting the sensors resonant frequency. This allows for characterizing the sensing layer in which the sensor is embedded. In the next section, an analytical method is described for the extraction of the complex permittivity of the sensing layer from the frequencies, $f_{D,max}$ and $f_{D,z}$, of the sensor, which can be obtained from measurement of the input admittance of the external antenna.

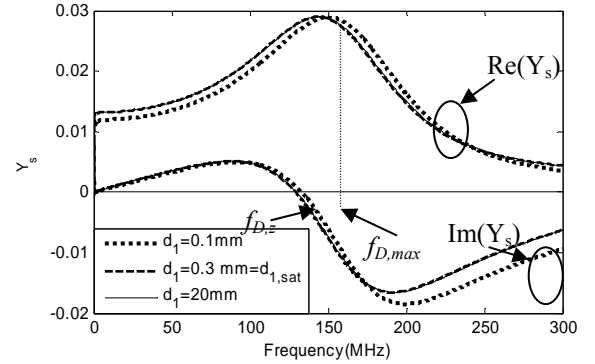


Fig. 8. Real part (conductance) and imaginary part (susceptance) of the admittance of the sensor in Fig.7 for different sensing layer thickness.

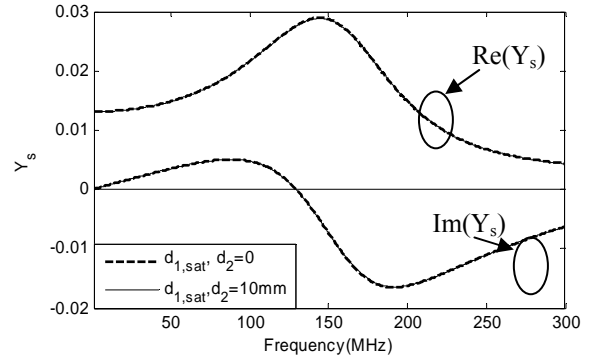


Fig. 9. Real part (conductance) and imaginary part (susceptance) of the admittance of the sensor in Fig.7 for two cases.

TABLE I
RESONANT FREQUENCIES OF LC SENSOR IN FIG.7 FOR DIFFERENT THICKNESSES AND OF SENSING LAYER AND ADDITIONAL LAYER

d_1 (mm)	d_2 (mm)	$f_{D,max}$ (MHZ)	$f_{D,z}$ (MHZ)
0.1	0	150.5	133.2
0.3 = $d_{1,sat}$	0	142.4	127.1

20 mm	0	142.5	127
$0.3 = d_{I,sat}$	10	142.3	126.8

IV. ANALYTICAL FORMULATION

In free space, the sensor resonant frequency, ω_A , and the sensor capacitance C_{sA} are given by the following.

$$\omega_A = \frac{1}{\sqrt{L_s C_{sA}}} \quad (6)$$

$$C_{sA} = \epsilon_0 (\epsilon_{rs} + 1)k \quad (7)$$

where k is defined in (3b).

The accurate measurement of lossy dielectric materials is challenging, especially when the conductivity becomes high [5]. In presence of a lossy dielectric, the equivalent circuit of the sensor is shown in Fig. 3 for which the admittance is defined as follows.

$$Y_s = \frac{1}{Z_s} = G_s + jB_s \quad (8)$$

From Z_s defined in (3), G_s and B_s can be simplified to the following form.

$$G_s = \frac{R_{sd}}{(R_{sd} - \omega^2 L_s R_{sd} C_{sd})^2 + (\omega L_s)^2} \quad (9)$$

$$B_s = \frac{\omega (R_{sd}^2 C_{sd} - \omega^2 L_s R_{sd} C_{sd}^2 - L_s)}{(R_{sd} - \omega^2 L_s R_{sd} C_{sd})^2 + (\omega L_s)^2} \quad (10)$$

The zero-susceptance angular frequency, $\omega_{D,z}$ and the maximum conductance angular frequency $\omega_{D,max}$ can be derived from (9) and (10) and written as follows.

$$\omega_{D,z} = \sqrt{\frac{1}{L_s C_{sd}} - \frac{1}{R_{sd}^2 C_{sd}^2}} \quad (11)$$

$$\omega_{D,max} = \frac{1}{C_{sd} R_{sd}} \sqrt{\frac{R_{sd}^2 R_{sd}^2 - L_s}{L_s}} \quad (12)$$

Substituting in (11) and (12) for C_{sd} and R_{sd} from (2), and for L_s from (6) and (7), the complex permittivity of sensing layer can be extracted and is given as follows,

$$\epsilon_{r1} = (\epsilon_{rs} + 1) \frac{\omega_A^2}{2\omega_{D,max}^2 - \omega_{D,z}^2} - \epsilon_{rs} \quad (13)$$

$$\sigma_1 = \epsilon_0 (\epsilon_{rs} + \epsilon_{r1}) \sqrt{2(\omega_{D,max}^2 - \omega_{D,z}^2)} \quad (14)$$

The zero-susceptance frequency $\omega_{D,max}$ is in general lower than $\omega_{D,z}$ and will decrease with increasing conductivity. This limits the maximum conductivity that

can be extracted using this method, to the value when $\omega_{D,z}$ becomes zero,

$$\sigma_{1,max} = \omega_A \epsilon_0 \sqrt{(\epsilon_{rs} + 1)(\epsilon_{rs} + \epsilon_{r1})} \quad (15)$$

It is dependent on the permittivity of the substrate ϵ_{rs} and the permittivity of the sensing layer, ϵ_{r1} as well as the resonant frequency, ω_A of the calibration measurement in free space. As compared to [5], the advantage of this technique is that it eliminates the approximation in the sensor geometry, using a reference such as free space.

V. RESULTS

A. Validation of the resonant frequency technique through Simulation

In this section, the resonant technique for determination of the complex permittivity of the sensing layer is verified with numerical results.

In the example considered, the substrate has a permittivity, ϵ_{rs} , equal to 2.33, and a thickness of 0.787 mm. The interdigital capacitor is designed with fingers of length 2.5 mm, width and spacing both equal to 62.5 μ m. There are a total of 10 fingers on each of the two electrodes. The loop inductor of the sensor has outer dimensions of 5 mm x 5 mm, while the resonant frequency of the calibration measurement in free space falls at $f_A = 812$ MHz.

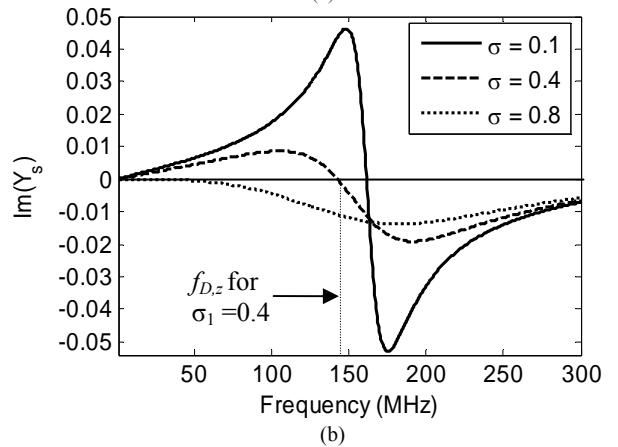
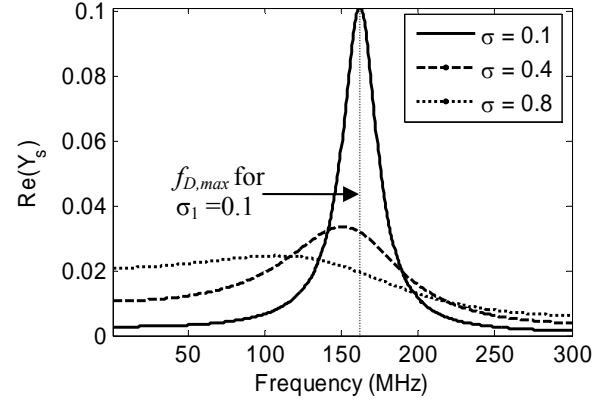


Fig. 10. (a) Real part and (b) imaginary part of the admittance of the sensor with a sensing layer with ϵ_{r1} equal to 80 and σ_1 varied.

The technique is first validated for the case where the sensing layer has a constant value for ϵ_{r1} equal to 80 and the conductivity σ_1 is varied. From the values of $f_{D,z}$ and $f_{D,max}$, the relative permittivity and conductivity of the sensing layer are extracted using the analytical expressions in (13) and (14). The maximum conductivity that can be extracted is determined using (15) and in this example, $\sigma_{1,max}$ is found to be equal to around 0.85 S/m. The real and imaginary parts of the admittance are shown in Fig.10 where the resonant frequencies are monitored for the different values of conductivity.

There is a good agreement between the extracted and expected relative permittivity values as shown in Table.2. It is noted that when the conductivity of the sensing layer became high, small discrepancies are found in extracting the permittivity values. This suggests that further parasitic elements, in particular for the loop inductor, probably need to be accounted for. However, since there is a large contrast between the properties of different biological tissues, the results still can be used for tissue differentiation, even for the high conductivity case.

TABLE II

EXTRACTION OF THE COMPLEX PERMITTIVITY OF A SENSING LAYER, OF PERMITTIVITY EQUAL TO 80, AND FOR DIFFERENT VALUES OF CONDUCTIVITY.

σ (S/m)	$f_{D,max}$ (MHZ)	$f_{D,z}$ (MHZ)	Extracted values		Extracted-Expected	
			ϵ_r	σ (S/m)	$\Delta\epsilon_r$	$\Delta\sigma$
0.1	160.6	160.2	82.4	0.08	2.4	0.02
0.2	158.6	156.6	82.8	0.17	2.8	0.03
0.3	155	150.2	83.9	0.26	3.9	0.04
0.4	149.7	140.6	85.3	0.35	5.3	0.05
0.5	142.5	127	87.3	0.46	7.3	0.04
0.6	133.2	107.5	89.4	0.57	9.4	0.03
0.7	120.3	77.3	93.3	0.69	13.3	0.01
0.8	108.2	22.6	93.5	0.80	13.5	0

B. Tissue Characterization

The sensing layer that encapsulates the sensor is next modeled to have dispersive electrical properties equivalent to those of biological tissues. The three types of sensing layers considered are representative of fat, liver and skin tissue. The complex permittivity profiles for these three types are taken from the measured tissue data available in the literature [6-8] and shown in Fig.11.

In each case, the resonant frequencies $f_{D,z}$ and $f_{D,max}$ are obtained, Table.3, from which the complex permittivities are extracted using (13) and (14). It is noted that for the case of the fat tissue, $f_{D,z}$ and $f_{D,max}$ are in the frequency

range where the relative permittivity and conductivity are relatively constant and the technique gives an accurate value for the permittivity. The extracted permittivity and conductivity of the fat layer are equal to 6.66 and 0.06 S/m respectively, and agree well with the dispersive values for the fat layer from [6-8]. For liver and wet skin, since the two frequencies are in the region where ϵ and σ are very dispersive, there is a greater discrepancy between the extracted and expected value. For example for the case of liver, the sensor in free space resonates at 812 MHz, and in the tissue $f_{D,z}$ and $f_{D,max}$ are at 130MHz and 145MHz, corresponding to the region where ϵ and σ are highly dispersive. If the sensor is designed to resonate at a much higher frequency in air to ensure that $f_{D,z}$ and $f_{D,max}$ are around 400MHz, very good agreement is expected. This shows the importance of the sensor design. However, the above demonstrates that this technique can characterize tissues.

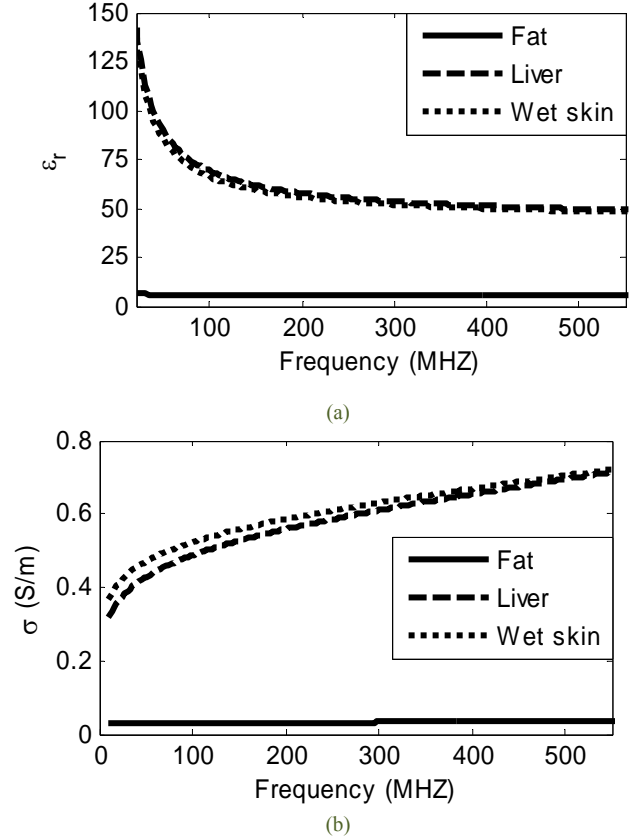


Fig. 11. (a) Relative permittivity ϵ_r and (b) conductivity σ as a function of frequency of fat, liver, and wet skin tissue [6-8].

TABLE III

EXTRACTION OF THE COMPLEX PERMITTIVITY OF A SENSING LAYER, OF PERMITTIVITY EQUIVALENT TO FAT TISSUE, LIVER TISSUE AND SKIN TISSUE THROUGH SIMULATION RESULTS.

Sensing	$f_{D,max}$	$f_{D,z}$	Extracted values	Expected values
---------	-------------	-----------	------------------	-----------------

layer	(MHZ)	(MHZ)	ϵ_r	σ (S/m)	ϵ_r	σ (S/m)
Fat	526.5	525.05	6.66	0.06	5.9	0.03
Liver	145	130	81.9	0.426	65	0.51
Wet Skin	145	121	72.04	0.47	60	0.55

A. Tissue Differentiation

In the following example, the sensor is embedded in a dispersive dielectric layer with electrical properties corresponding to normal breast tissue, and compared to the case when it is embedded in cancerous breast tissue. The goal is to differentiate between the two tissue types using the extracted material properties. The permittivity profile of the sensing dielectric layers is taken from the literature [13] for measurements of normal and cancerous breast tissues obtained from patients undergoing surgical mastectomy and are shown in Fig.12.

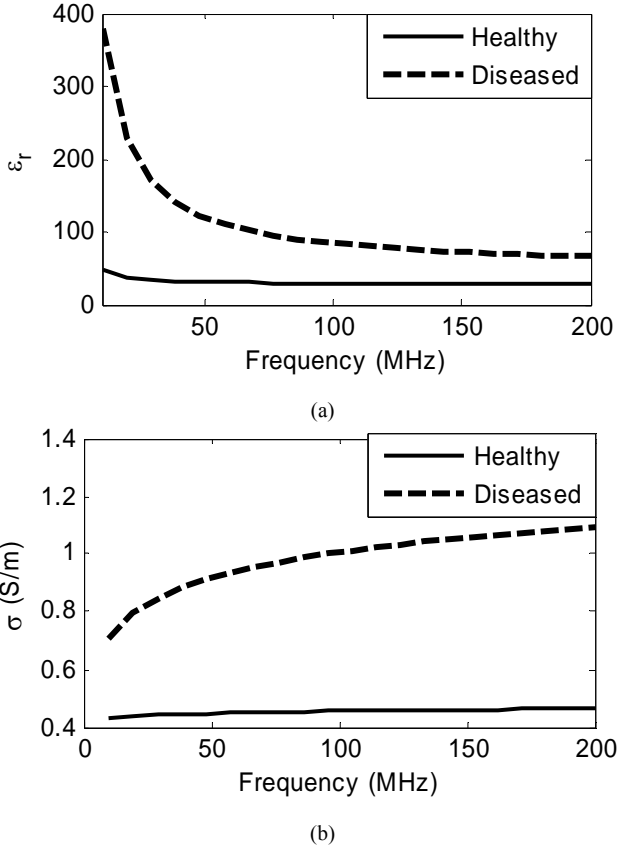


Fig. 12. (a) Relative permittivity ϵ_r and (b) conductivity σ as a function of frequency of healthy breast tissue (adipose) and diseased tissue (tumor) [13].

The results obtained are summarized in Table.4. This technique retrieves the material properties in the small frequency range between $f_{D,z}$ and $f_{D,max}$. For diseased tissue, the resonant frequencies are at 49MHz and 64MHz (Table.4), where the relative permittivity profile is highly dispersive as seen in Fig.12.a. This explains the high discrepancy in the extraction of the relative permittivity obtained in Table.4.

Once again, the importance of the sensor design is demonstrated. The sensor should be designed to have a higher resonant frequency inside tissue. However, because of the high contrast between the healthy and diseased tissue the discrepancy between the extracted and expected relative permittivities and conductivities is not much and the methodology is sufficient to differentiate between the tissues.

TABLE IV
EXTRACTION OF THE COMPLEX PERMITTIVITY OF A SENSING LAYER, OF PERMITTIVITY EQUIVALENT TO HEALTHY DISEASED BREAST TISSUE THROUGH SIMULATION RESULTS.

Sensing layer	$f_{D,max}$ (MHZ)	$f_{D,z}$ (MHZ)	Extracted values		Expected values	
			ϵ_r	σ (S/m)	ϵ_r	σ (S/m)
Diseased	68	49	314.7	1.1	115	0.95
Healthy	184	105.8	35.6	0.44	30	0.43

B. Extraction of Permittivity through Experimentation

All of the above has been demonstrated through experimentation with a telemetry consisting of a fabricated transmit/receive loop antenna and a prototype LC circuit immersed in single and multiple dispersive regions. Prototype sensors with a planar square inductor in series with an interdigital capacitor have been fabricated as shown in Fig.13, on Rogers RT/duroid 5880 ($\epsilon_r = 2.22$) substrate of thickness equal to 1.575 mm. The dimensions of the three sensors are listed in Table.5. Various size of sensors ranging from 20mm x 20 mm, to 5mmx5mm have been analyzed to show the importance of the sensor design, and their resonant frequencies when implanted in tissue phantom. **Although these sizes are consistent with previous study of implantable devices [14,15], future work will explore the miniaturization of the device as well as investigation of the biocompatibility of the device for long term implantation.**

TABLE V
DIMENSION OF PROTOTYPE LC SENSOR FABRICATED

LC sensor size	Inductor parameters	IDC parameters
20 mm x 20 mm	7.5 turns w = 250mm s = 250mm	N = 19 w = 250mm s = 250mm
10 mm x 10 mm	7.5 turns w = 125mm s = 125mm	N = 9 w = 125mm s = 125mm
5mm x 5mm	3.5 turns w = 125mm s = 125mm	N = 3, w = 100mm s = 100mm

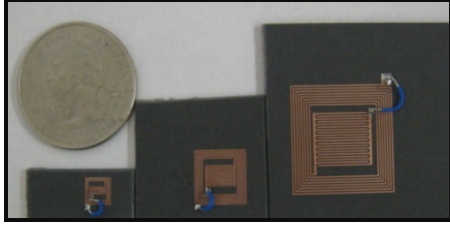


Fig. 13. Picture of fabricated LC sensors of dimensions 5mm x5mm, 10mm x 10mm, and 20mm x 20mm on Duroid 5880 ($\epsilon_{rs}=2.22$, $h=1.575$ mm).

The resonant frequency of the sensor is obtained by measuring the input impedance of the antenna, connected to the Agilent 8753D network analyzer as shown in Fig.14. The external antenna is designed to have a diameter approximately equal to the diameter of the sensor and has between 3 to 4 turns. The communication between the antenna and sensor is optimized in free space by minor adjustment to the antenna dimensions.

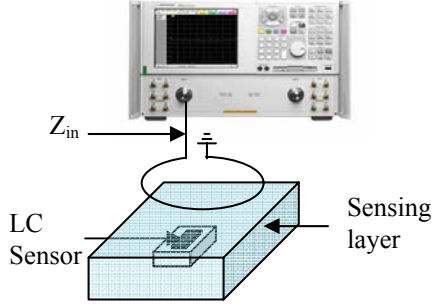


Fig.14. Experimental setup.

A calibration measurement is performed in free space to determine its self-resonant frequency, at which the zero-susceptance and maximum conductance frequencies are the same. Once encapsulated within a biological tissue, these frequencies will shift. The impact of embedding the sensor in multiple dispersive layers has first been investigated in Fig.15. Two different configurations have been compared; a single layer of de-ionized water with a thickness of 5 mm, and two layers consisting of de-ionized water (2 mm thick) and oil (5 mm thick). It is seen that there is a shift in the resonant frequency of the sensor and that there is no additional shift when the second layer is added, demonstrating that only the first layer impacts the resonant frequency shift.

For validation, the complex dielectric permittivity of the deionized water is also measured with the Agilent 85070E high temperature probe and the E4191A Impedance Analyzer [16]. Table.6 summarizes the results of the material property extraction. The extraction technique using the telemetry link compares well with the measured values obtained from the Agilent 85070E high temperature probe.

TABLE VI
MEASUREMENTS OF DEIONIZED WATER

	ϵ_r	σ (S/m)
85070E Agilent probe	79	0.0011
Measured results	81.2	0.0016

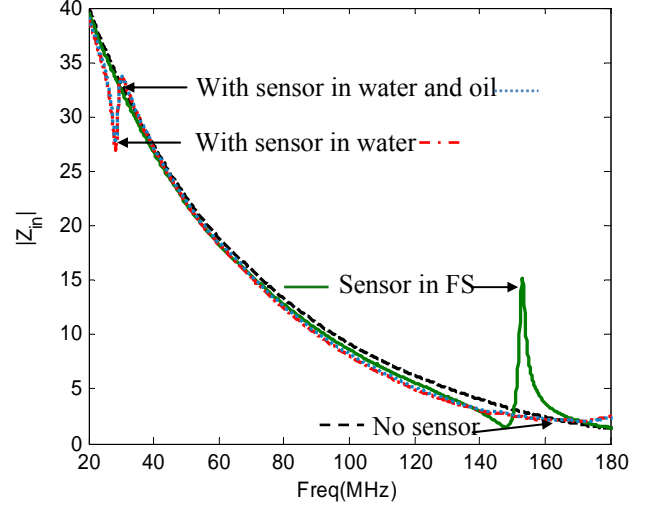


Fig. 15. Measured magnitude of the input impedance of the antenna isolated from the sensor and in proximity of the sensor in free space and inside water.

C. Experimental Validation using Phantom Tissues

Based on [17], a phantom model representative of fat has been fabricated. The fat phantom was composed of 3% of NaCl solution (0.9% NaCl, 99.1% H₂O water), 30% of corn oil and 67% of flour. The dielectric permittivity of the phantoms was first measured with the Agilent 85070E high temperature probe and the E4191A Impedance Analyzer. The sensors shown in Fig.13 were embedded inside the fabricated phantom materials. In each case the external antenna is used to measure the resonant frequencies and the results are summarized in Table.7. From the measured resonant frequencies $f_{D,z}$ and $f_{D,max}$, as well as that in free space f_A , the relative permittivity and conductivity of the phantom layer are extracted using the analytical expressions developed in the previous section. The extracted results from the measurements correspond to the values of the complex permittivity at the resonant frequencies. The results are compared to the measurement from the dielectric probe measurements. They show good agreement.

TABLE VII
EXTRACTION OF THE COMPLEX PERMITTIVITY OF FAT PHANTOM LAYER THROUGH MEASUREMENT RESULTS

LC	$f_{D,max}$ (MHZ)	$f_{D,z}$ (MHZ)	Extracted values (This technique)	Expected values (Agilent Dielectric Probe)

			ϵ_r	σ (S/m)	ϵ_r	σ (S/m)
20 mm x 20 mm	33.4	33.35	7.27	0.0014	8	0.0007
10 mm x 10 mm	81.9	81.7	6.54	0.004	7.5	0.001
5 mm X 5 mm	400.5	400.3	5.34	0.0075	6.4	0.005

The sensor that has a resonant frequency in free space, f_A , equal to 150 MHz is now used to differentiate two tissues types, mainly low water content and high water content tissue. The sensor is embedded in the fat phantom layer, and compared to the case when it is embedded in a phantom with properties corresponding to a muscle tissue layer. The muscle phantom [17] was composed of 35% of NaCl solution (0.9% NaCl, 99.1% H₂O water), 21% of deionized water, 40% of sugar and 4% of technical agar.

The goal is to differentiate between the two tissue types using the extracted material properties. In each case the external antenna is used to measure the resonant frequencies and the results are summarized in Table.8. From the measured resonant frequencies $f_{D,z}$ and $f_{D,max}$, as well as that in free space f_A , the relative permittivity and conductivity of the phantom layer are extracted using the analytical expressions developed in the previous section. Again, the results are compared to the direct measurements using the dielectric probe. Discrepancies are observed for the conductivity extraction of the muscle phantom. However, the extraction of the relative permittivity show good agreement for both tissue types. The experiment again demonstrates that this technique can characterize tissue types.

TABLE VIII
CHARACTERIZATION OF TISSUES USING FAT AND MUSCLE TISSUE
PHANTOMS THROUGH MEASUREMENT RESULTS

Tissue	$f_{D,max}$ (MHZ)	$f_{D,z}$ (MHZ)	Extracted values (This technique)		Expected values (Agilent Dielectric Probe)	
			ϵ_r	σ (S/m)	ϵ_r	σ (S/m)
Fat	81.9	81.7	6.54	0.004	7.5	0.001
Muscle	29.5	28.5	97	0.3	86	0.5

VI. CONCLUSIONS

The major focus of this work has been to develop a technique for tissue characterization and differentiation based on the contrast in the electrical properties between tissues and for the same tissue in healthy and diseased states. The RF telemetry consists of an LC sensor embedded in tissue and communicating with an external antenna by inductive coupling. A resonant frequency

technique has been developed for extracting the electrical properties of the tissue in which the sensor is embedded. The extraction of complex permittivity is based on measurements that can be made by the external antenna. Using an equivalent circuit model of the sensor that accounts for the properties of the encapsulating tissue, analytical expressions have been developed for the extraction of the tissue permittivity and conductivity.

Before embedding the sensor in tissue, a calibration procedure is done where the sensor resonant frequency is noted. This eliminates the inductance and all parasitic capacitances in the final analytical expression. With the sensor now embedded in tissue, the frequencies at which the sensor conductance becomes a maximum and at which the susceptance becomes zero are noted. These frequencies have been correlated to the electrical characteristics of the tissues. The technique has been validated for tissue characterization with the sensor embedded in several configurations of multilayered tissue with typical values for thicknesses and complex permittivities. Since the resonant frequencies respond very well to the contrast in electrical characteristics, this technique shows great promise for tissue characterization and differentiation. The first step toward the development of the sensor has been demonstrated. **Future work includes miniaturization of the device and fabrication with fully bio-compatible materials. Finally, experimental validation will be done with the help of measurements with dead then live animal tissue, and clinical studies on human tissue.**

ACKNOWLEDGEMENTS

The authors thank Benjamin Freer for his assistance with the phantom fabrication and measurements.

REFERENCES

- [1] W. Greatbatch and C. F. Holmes, "History of Implantable Devices," *IEEE Eng. in Med. and Biol.*, vol. 10, 1991, pp. 38-49.
- [2] W.T. Chen and H.R. Chuang, "Numerical computation of the EM coupling between a circular loop antenna and a full-scale human-body model," *IEEE Trans. Micr. Th. Tech.*, vol. 46, 1998, pp. 1516-1520.
- [3] F. A Miranda and R.N. Simons, "Validation of Radio Frequency Telemetry Concept in the Presence of Biological Tissue-Like Stratified Media," *IEEE Ant Prop Soc Inter Symp Digest.*, vol. 2, 2004, pp. 1335-1338.
- [4] M. Yvanoff, J. Venkataraman, L. Fuller, "Impact of multiple tissue layers on an implantable LC sensor," *Microwave an Optical Technology Letters*, vol. 50, March 2008, pp.783-787.
- [5] K.G. Ong, C.A. Grimes, C.L. Robbins, R.S. Singh, "Design and application of a wireless, passive, resonant-circuit environmental monitoring sensor," *Sensors and Actuators A*, vol. 93, Feb 2001, pp. 33-43.
- [6] C. Gabriel, S. Gabriel and R. Corthout "The dielectric properties of biological tissues:I.Litterature survey," *Phys. Med. Biol.*, vol. 41,1996.

- [7] S. Gabriel, R.W. Lau and C. Gabriel "The dielectric properties of biological tissues:II.Measurements in the frequency range 10Hz to 20GHz," *Phys. Med. Biol.*, vol. 41,1996.
- [8] S. Gabriel, R.W. Lau and C. Gabriel "The dielectric properties of biological tissues:III.Parametric models for the dielectric spectrum of tissues," *Phys. Med. Biol.*, vol. 41,1996.
- [9] S. S. Mohan, M. delMar Hershenson, T.H.Lee, "Simple accurate expressions for planar spiral inductances," *IEEE Solid-State Circuits*, vol. 34, Oct. 1999, pp. 1419-1424.
- [10] S. S. Gevorgian, T. Martinson, P.L.J. Linner, E.L. Kollberg, "CAD models for multilayered substrate Interdigital capacitors," *IEEE Trans. Micr. Th. Tech.*, vol. 44, 1996, pp. 896-904.
- [11] <http://www.sonnetusa.com>
- [12] J.S Kim, D.G. Lee," Analysis of dielectric sensors for the cure monitoring of resin matrix composite materials," *Sensors and Actuators B*, vol. 30, 1996, pp. 159-164.
- [13] M.R.Stoneman, M. Kosempa, W.D. Gregory, C.W. Gregory, J.J. Marx, W. Mikkelson, J. Tjoe and V. Raicu, "Correction of electrode polarization contributions to the dielectric properties of normal and cancerous breast tissues at audio/frequencies," *Phys. Med. Biol.*, vol. 52, 2007, pp. 6589-6604.
- [14] Karacolak, T. Hood, A.Z. Topsakal, E., "Design of a Dual-Band Implantable Antenna and Development of Skin Mimicking Gels for Continuous Glucose Monitoring" *IEEE Trans. Micro. The. Tech.*, Vol. 8, April 2008.
- [15] Alec Ginggen, Yanik Tardy, Rocco Crivelli, Toralf Bork, and Philippe Renaud, "A Telemetric Pressure Sensor System for Biomedical Applications", *IEEE Trans. On Bio. Eng.*, vol. 55, April 2008.
- [16] <http://www.home.agilent.com>
- [17] A. Gund and S. Lindqvist, "Phantom Making and Modeling of Monopole Antennas in FD-TD for Breast Cancer Studies Department of Signals and Systems," Chalmers University of Technology, Sweden, 2005.
- [18] K. Ito, "Human Body Phantoms for Evaluation of Wearable and Implantable Antennas", *The Second Eur. Conf. On Antennas and Propagation*, Nov. 2007.
- [19] E.Zastrow, S.K Davis, M. Lazbnik, F. Kelcz, B.D VanVeen, S.C. Hagness, "Development of Anatomically Realistic Numerical Breast Phantoms with Accurate Dielectric Properties for Modeling Microwave Interactions with the Human Breast," *IEEE Trans. on Bio. Eng.* , Oct. 2008, Accepted for publication.